Error Performance of Pulse-Based Ultra-Wideband MIMO Systems Over Indoor Wireless Channels

Huaping Liu, *Member, IEEE*, Robert C. Qiu, *Senior Member, IEEE*, and Zhi Tian, *Member, IEEE*

***Abstract*—Multiple-input multiple-output (MIMO) techniques are applied to ultrawideband (UWB) systems to achieve high-rate communications over indoor wireless channels. The receiver employs a zero-forcing (ZF) scheme to separate N parallel transmitted data streams for each resolvable multipath component. A RAKE is then applied to combine the ZF paths carrying information of the same symbol to form the decision variable. Analytical error rate expression of an (N, M, L) system (N transmit antennas, M receive antennas, and L paths combined) over a pragmatic indoor log-normal fading channel is derived, which captures the diversity order by a single degree-of-freedom parameter.**

***Index Terms*—Log-normal fading, multiple antennas, performance analysis, ultrawideband.**

I. Introduction

ULTRA-WIDEBAND (UWB) [1]–[8] has attracted significant academic and commercial interest because of its capability to overlay spectrum with legacy narrowband radios and its potential to deliver high data rates over short distances. A widely used UWB scheme is pulse based, which employs short-duration low-duty-cycle pulses to transmit information. However, the transmission rate of such signaling is limited by the channel excess delay in order to avoid excessive intersymbol interference (ISI). In addition, the low transmission power limits the system RF range.

Multiple antennas have been used in the reverse link of mobile communication systems to suppress or cancel interference [9], [10] and to achieve transmit or receive diversity. Multiple-input multiple-output (MIMO) systems [11]–[13] use multiple antennas at both ends of the wireless link and have been shown to provide high spectral efficiencies. MIMO techniques can be applied to UWB systems to extend system RF range through spatial diversity, to increase throughput that is limited by the channel excess delay through spatial multiplexing, and to cancel potential narrowband interference. Existing research on MIMO systems has focused mostly on detection, performance analysis, and theoretical capacity in frequency-nonselective Rayleigh fading environments. In [14], performance of UWB MIMO systems over Rayleigh fading channels with additive white Gaussian noise (AWGN) was studied by simulations. In [15], a UWB multiple-antenna transceiver architecture was suggested for fourth-generation wireless LAN systems. In [16], the bit error rate (BER) of a UWB system employing pulse-position modulation (PPM) was studied using an array model [17]. Major applications of UWB are likely to be for indoor environments for which the channel amplitude exhibits log-normal fading [18], [19] rather than the well-addressed Rayleigh fading. It is a meaningful yet nontrivial task to find an analytical approach to deal with log-normal fading, which has not been addressed in the literature. There is a need to investigate UWB MIMO systems in pragmatic indoor wireless environments.

In this paper, the analytical error performance of MIMO systems over highly frequency-selective UWB log-normal fading channels is analyzed. A zero-forcing (ZF) scheme is used to separate the spatially multiplexed data on a path-by-path basis. Then, a temporal RAKE receiver employing maximal ratio combining (MRC) is applied to the ZF paths to form the decision statistics. The rest of the paper is organized as follows. The UWB MIMO system model is given in Section II. Receiver performance is analyzed in Section IV. In Section V, we provide numerical results, followed by concluding remarks in Section VI.

II. System Model

A. Transmitted Signal

Consider a communication system consisting of N transmit and M receive antennas that operates over a UWB channel. Input data are serial-to-parallel converted into N streams without space–time encoding. Each of the N streams of symbols is then used to modulate (the pulse amplitude of) a short-duration UWB pulse. Finally, the N streams of waveforms are distributed to N transmit antennas for simultaneous transmission. Each receive antenna responds to each transmit antenna through statistically independent fading processes. The received signals are further corrupted by AWGN that is statistically independent among the M receiver antennas and across different symbol periods as well as different resolvable paths of the same symbol.

Manuscript received December 26, 2003; revised November 6, 2004; accepted November 10, 2004. The editor coordinating the review of this paper and approving it for publication is A. Molisch. The work of Z. Tian was supported by the National Science Foundation under Grants CCR-0238174 and ECS-0427430.

H. Liu is with the School of Electrical Engineering and Computer Science, Oregon State University, Corvallis, OR 97331 USA (e-mail: hliu@eecs.orst.edu).

R. C. Qiu is with the Department of Electrical and Computer Engineering, Tennessee Technological University, Cookeville, TN 38505 USA.

Z. Tian is with the Department of Electrical and Computer Engineering, Michigan Technological University, Houghton, MI 49931-1295 USA.

Digital Object Identifier 10.1109/TWC.2005.858350

The transmitted PAM signal from the nth transmit antenna is expressed as

$$x_n(t) = \sum_{k=-\infty}^{\infty} \sqrt{E_s} s_n(k) p(t - k\mathcal{T}_r) \tag{1}$$

where $s_n(k)$ is the kth information symbol[1] from the nth transmit antenna, E_s is the energy of the basic pulse $p(t)$ or equivalently the average energy per symbol, and $\mathcal{T}_r$ is the pulse repetition interval (PRI). The unit energy UWB pulse $p(t)(\int_{-\infty}^{\infty} p^2(t)dt = 1)$ has a very narrow nonzero time support $\mathcal{T}_p \ll \mathcal{T}_r$, resulting in low duty cycle transmission. To avoid severe ISI,[2] $\mathcal{T}_r$ must be sufficiently large compared with the channel delay spread experienced.

B. Received Signal

Pulse-based UWB signaling gives rise to highly frequency-selective channels. Thus, the energy of the received signal is scattered over a number of resolvable multipath components. Adopting the statistical channel model in this paper, we describe the channel impulse response as [3], [18], [20]

$$c(t) = \sum_{l=0}^{L_r-1} h(l)\delta(t - l\mathcal{T}_p) \tag{2}$$

where L_r is the total number of resolvable multipath components, $\delta(t)$ is the Dirac delta function, $\mathcal{T}_p$ is the minimum multipath resolution, and $h(l)$ represents the fading coefficient of the lth resolvable path whose magnitude follows a log-normal distribution. The minimum multipath resolution $\mathcal{T}_p$ is equal to the duration of $p(t)$, as any two paths whose relative delay is less than the pulse duration are not resolvable. The channel fading coefficient $h(l)$ can be modeled as [19] $h(l) = \varepsilon(l)\alpha(l)$, where $\alpha(l)$ is the log-normal fading magnitude term and $\varepsilon(l) \in \{-1, 1\}$ with equal probability represents the random pulse-phase inversion that may occur due to reflection [19]. The average power of path l is represented by $\mathrm{E}\{|h(l)|^2\} = \Omega_0 e^{-\rho l}$, where $\mathrm{E}\{\cdot\}$ denotes expectation, Ω_0 is a scalar for normalizing the power contained in resolvable paths, and ρ is the power decay factor.

Practical values of L_r depend on the rms delay spread of the channel τ_{rms}, multipath resolution, and the range of attenuation from the statistically strongest path to the weakest path considered. In [19], it was reported that with $\tau_{\mathrm{rms}} = 25$ ns and $\mathcal{T}_p = 0.167$ ns, the average number of resolvable paths (within a 10-dB range) is about $L_r = 41$.

To maintain reasonable system complexity, however, it is impractical to combine all resolvable paths. Thus, it is assumed in the rest of this paper that only a subset of $L(L \le L_r)$ resolvable paths will be exploited by the receiver for symbol detection. Signals from each transmit antenna go through the multipath channel modeled by (2), resulting in multiple delayed and independently faded copies of the same signal aggregated at the receiver. The received signal $r_m(t)$ at the mth receive antenna $m = 1, \ldots, M$ is a sum of signals from all N transmit antennas expressed as

$$r_m(t) = \sum_{n=1}^{N} \sum_{l=0}^{L-1} h_{mn}(l) x_n(t - l\mathcal{T}_p) + \nu_m(t) \tag{3}$$

where $h_{mn}(l)$ represents the fading coefficient of the lth path for the signal from the nth transmit antenna to the mth receive antenna, $\nu_m(t)$ is a real zero-mean white Gaussian noise process with a two-sided power spectral density of $N_0/2$, and $x_n(t)$ was given in (1).

The receiver consists of a matched filter matched to the UWB pulse $p(t)$ and then sampled at each path interval. The output of the matched filter is processed by an array processing unit to separate signals from N transmit antennas on a path-by-path basis. A RAKE receiver is then used to combine the ZF paths carrying information of the same symbol and form the decision statistics for a symbol-by-symbol detection.

Mathematical models for such a detection procedure can be briefly described as follows. Over each symbol period, N symbols are sent over N transmit antennas to form an $N \times 1$ transmit signal vector $\boldsymbol{s} = [s_1, s_2, \ldots, s_N]^T$. Corresponding to the lth propagation path, the received $M \times 1$ spatial signal vector at the matched filter output $\boldsymbol{r}(l)$ is represented by

$$\boldsymbol{r}(l) = [r_1(l),\ r_2(l),\ \ldots,\ r_M(l)]^T, \quad l = 0, \ldots, L-1 \tag{4}$$

where $[\cdot]^T$ denotes transpose. Within $\boldsymbol{r}(l)$, the received noise vector across M receive antennas $\boldsymbol{\nu}(l)$ is expressed as

$$\boldsymbol{\nu}(l) = [\nu_1(l),\ \nu_2(l),\ \ldots,\ \nu_M(l)]^T, \quad l = 0, \ldots, L-1. \tag{5}$$

For the lth delayed path, the discrete-time channel gains among all pairs of transmit receive antennas can be organized into an $M \times N$ matrix $\boldsymbol{H}(l)$

$$\begin{aligned} \boldsymbol{H}(l) &= [\boldsymbol{h}_1(l)\, \boldsymbol{h}_2(l)\, \cdots\, \boldsymbol{h}_N(l)] \\ &= \begin{bmatrix} h_{11}(l) & h_{12}(l) & \cdots & h_{1N}(l) \\ h_{21}(l) & h_{22}(l) & \cdots & h_{2N}(l) \\ \vdots & & & \vdots \\ h_{M1}(l) & h_{M2}(l) & \cdots & h_{MN}(l) \end{bmatrix} \end{aligned} \tag{6}$$

where the $M \times 1$ column vector $\boldsymbol{h}_n(l)$ is given as $\boldsymbol{h}_n(l) = [h_{1n}(l)\, h_{2n}(l)\, \cdots\, h_{Mn}(l)]^T$.

Based on the channel model in (2), there is no interpath interference for data from the same transmit antenna. Thus, the received signal can be modeled on a path-by-path basis. Assuming perfect timing and synchronization, the received spatial signal vector $\boldsymbol{r}(l)$ in (4) can now be written in a vector-matrix form as[3]

$$\boldsymbol{r}(l) = \sqrt{E_s}\boldsymbol{H}(l)\boldsymbol{s} + \boldsymbol{\nu}(l), \quad l = 0, \ldots, L-1 \tag{7}$$

[1]The average energy of the signal constellation should be normalized to unity.

[2]The level of ISI is typically determined by the channel rms delay spread for a given pulse repetition frequency.

[3]This is based on the assumption that PRI $\mathcal{T}_r$ is sufficiently large compared to the channel delay spread so that there is no ISI.

where the noise vector $\boldsymbol{\nu}(l)$ is independent of channel fading processes. When more realistic timing and synchronization are considered [7], [8], (7) needs modifications, but the mathematical structure of this paper is still valid. When per-path pulse distortion is included in the channel model [4], [5], a generalized version of the RAKE structure can be used. In the generalized RAKE, the receiver consists of a matched filter matched to the distorted UWB pulse of the lth path and the mathematical model given in (7) still has the same form.

III. Detection

For spatial processing, the ZF scheme is adopted in this paper to separate data streams from N transmit antennas on a path-by-path basis. Performance of the ZF scheme approaches that of the minimum mean square error (MMSE) scheme at high signal-to-noise ratios [9], and it is convenient to analyze the ZF structure. In the ZF receiver, the received signal vector in (7) is premultiplied by $\boldsymbol{H}(l)^+$, where $(\cdot)^+$ denotes the pseudoinverse. Thus, the ZF $N \times 1$ signal vector $\boldsymbol{y}(l)$ for the lth path of a particular symbol can be written as

$$\begin{aligned}\boldsymbol{y}(l) &= [y_1(l),\ y_2(l),\ \ldots,\ y_N(l)]^T \\ &= \boldsymbol{H}(l)^+\boldsymbol{r}(l) = \sqrt{E_s}\boldsymbol{s} + \boldsymbol{\xi}(l) \end{aligned} \tag{8}$$

where $\boldsymbol{\xi}(l) = \boldsymbol{H}(l)^+\boldsymbol{\nu}(l)$ is the zero-mean noise vector. The instantaneous noise power (conditioned on a fixed realization of channel coefficients) on the lth path of the nth data stream is obtained as

$$\left[\mathrm{E}\left\{\boldsymbol{\xi}(l)\boldsymbol{\xi}(l)^H\right\}\right]_{nn} = \left(\frac{N_0}{2}\right)\left[\boldsymbol{H}(l)^+\boldsymbol{H}(l)^{+H}\right]_{nn}$$

where $(\cdot)^H$ denotes conjugate transpose[4] and $[\cdot]_{nn}$ represents the (n,n)th element of a matrix. If $\boldsymbol{H}(l)^H\boldsymbol{H}(l)$ is a full rank matrix,[5] the relation can be easily obtained as

$$\left[\mathrm{E}\left\{\boldsymbol{\xi}(l)\boldsymbol{\xi}(l)^H\right\}\right]_{nn} = \left(\frac{N_0}{2}\right)\left[\left(\boldsymbol{H}(l)^H\boldsymbol{H}(l)\right)^{-1}\right]_{nn}. \tag{9}$$

For notational simplicity, let us introduce a new variable

$$\kappa_n(l) = \frac{1}{\sqrt{\left[\left(\boldsymbol{H}(l)^H\boldsymbol{H}(l)\right)^{-1}\right]_{nn}}}. \tag{10}$$

It was shown in [9] that $\kappa_n(l)^2 = 1/[(\boldsymbol{H}(l)^H\boldsymbol{H}(l))^{-1}]_{nn}$ can be written in quadratic form as

$$\kappa_n^2(l) = \boldsymbol{h}_n(l)^H\boldsymbol{G}(l)\boldsymbol{h}_n(l) \tag{11}$$

where $\boldsymbol{h}_n(l)$ was defined in (6) and $\boldsymbol{G}(l)$ is an $M \times M$ positive semidefinite Hermitian matrix formed from $\boldsymbol{h}_1(l), \ldots, \boldsymbol{h}_{n-1}(l), \boldsymbol{h}_{n+1}(l), \ldots, \boldsymbol{h}_N(l)$, and thus is independent of $\boldsymbol{h}_n(l)$. For example, with $N = 2$ and $n = 1$, $\boldsymbol{G}(l)$ is determined to be $\boldsymbol{G}(l) = \boldsymbol{h}_2(l)^T\boldsymbol{h}_2(l)\boldsymbol{I}_2 - \boldsymbol{h}_2(l)\boldsymbol{h}_2(l)^T$, where $\boldsymbol{I}_2$ is the 2×2 identify matrix.

Mathematically, it is possible to detect the transmitted signal $\boldsymbol{s}$ from the spatial-processed received signal in (8) that corresponds to a single path in any chip interval. However, for better performance, the receiver should temporally combine the signal energy contained in many resolvable paths corresponding to a particular symbol. From (8), we collect the ZF signal elements from all L paths carrying the same symbol of the nth data stream and write them in an $L \times 1$ temporal vector as

$$\begin{aligned}\boldsymbol{y}_n &= [y_n(0),\ y_n(1),\ \ldots,\ y_n(L-1)]^T \\ &= \left[\sqrt{E_s}s_n + \xi_n(0),\ \ldots,\ \sqrt{E_s}s_n + \xi_n(L-1)\right]^T. \end{aligned} \tag{12}$$

The decision variable for a symbol from the nth transmit antenna can be obtained by combining the L elements of $\boldsymbol{y}_n$. The MRC output for a particular symbol of the nth transmitted data stream is expressed as a single decision variable of the form

$$d_n = \sum_{l=0}^{L-1}\kappa_n^2(l)\left[\sqrt{E_s}s_n + \xi_n(l)\right]. \tag{13}$$

IV. Error Performance

While the model in Section II applies to a general PAM system, our performance analysis will focus on the binary PAM scheme. Correspondingly, the average symbol energy E_s will be replaced by the bit energy E_b in the following analysis. The performance results can be easily extended to a general PAM scheme. Let us examine the error behavior of the transmitted bit s_n. For notational simplicity, the subscript n indexing the nth data stream for some variables (e.g., in $\kappa_n(l)$ and $\boldsymbol{h}_n(l)$) will be omitted whenever it does not cause a confusion. Notice that with polar PAM signaling and the channel model adopted, both the signal component and the noise component are real valued. For a fixed set of $\{\kappa(l)\}$, or equivalently a fixed realization of channel coefficients $\{\boldsymbol{H}(l)\}$, the instantaneous SNR γ_p of the decision variable in (13) can be written as

$$\gamma_p = \frac{2E_b}{N_0}\sum_{l=0}^{L-1}\kappa^2(l). \tag{14}$$

The conditional BER expression conditioned on a fixed set of channel coefficients is given as

$$P(\gamma_p) = Q(\sqrt{\gamma_p}) \tag{15}$$

where $Q(x) = (1/\sqrt{2\pi})\int_x^\infty e^{-y^2/2}dy$ is the complementary error Q-function.

[4]For the channel model adopted in this paper, all channel coefficients are real. The notation of conjugate transpose is still kept when operating on real vectors or matrices because of its mathematical convenience.

[5]Such a condition is usually satisfied when signals from transmit and receive antennas are independent or have low correlations, which is assumed true in this paper.

In order to derive the average BER, we need the probability density function (pdf) of γ_p. Substituting (11) into (14) yields

$$\gamma_p = \gamma_0 \sum_{l=0}^{L-1} \boldsymbol{h}(l)^H \boldsymbol{G}(l) \boldsymbol{h}(l)$$

where $\gamma_0 = 2E_b/N_0$. Let us form an $LM \times LM$ matrix $\boldsymbol{G}$ and an $LM \times 1$ vector $\boldsymbol{h}$ as

$$\boldsymbol{G} = \text{diag}\left[\boldsymbol{G}(0)\ \boldsymbol{G}(1)\ \cdots\ \boldsymbol{G}(L-1)\right] \tag{16}$$

$$\boldsymbol{h} = \left[\boldsymbol{h}(0)^T\ \boldsymbol{h}(1)^T\ \cdots\ \boldsymbol{h}(L-1)^T\right]^T \tag{17}$$

where $\boldsymbol{h}(l) = [h_1(l)\ h_2(l)\ \cdots\ h_M(l)]^T, l = 0, \ldots, L-1$. The instantaneous SNR γ_p can now be written in quadratic form as

$$\gamma_p = \gamma_0 \boldsymbol{h}^H \boldsymbol{G} \boldsymbol{h} \tag{18}$$

where $\boldsymbol{G}$, being a Hermitian matrix, can be diagonalized in the form [21]

$$\boldsymbol{G} = \boldsymbol{U} \boldsymbol{\Lambda} \boldsymbol{U}^H. \tag{19}$$

Here, $\boldsymbol{U}$ is a unitary matrix (i.e., $\boldsymbol{U}\boldsymbol{U}^H = \boldsymbol{U}^H\boldsymbol{U} = \boldsymbol{I}_{LM}$) and

$$\boldsymbol{\Lambda} = \text{diag}[\lambda_1,\ \ldots,\ \lambda_{LM}] \tag{20}$$

is a diagonal matrix whose diagonal elements $\lambda_1,\ \ldots,\ \lambda_{LM}$ are the eigenvalues of matrix $\boldsymbol{G}$. Therefore, γ_p can be expressed as a diagonal Hermitian form with independent variates as

$$\gamma_p = \gamma_0 \boldsymbol{f}^H \boldsymbol{\Lambda} \boldsymbol{f} = \gamma_0 \gamma_p' \tag{21}$$

where

$$\boldsymbol{f} = [f_1, \ldots, f_{LM}]^T = \boldsymbol{U}^H \boldsymbol{h}. \tag{22}$$

Since elements of the zero-mean vector $\boldsymbol{h}$ are independent of elements of $\boldsymbol{G}$, $\boldsymbol{f}$ is obviously also a zero-mean vector.

The key in evaluating the analytical performance of a MIMO UWB system is to derive the statistics of $\boldsymbol{f}$, which is difficult to obtain for a log-normal fading channel. For practical implementation constraints, the number of paths to be combined (L) is typically small (e.g., less than 10). Hence, among all paths combined by the MRC, the average power of the weakest path is approximately equal to the average power of the strongest path. To simplify the analysis, we assume that all L paths combined by the receiver have equal power (i.e., $\rho = 0$) and $\Omega_0 = 1$. Thus, $\mathrm{E}\{\boldsymbol{h}\boldsymbol{h}^H\} = \text{diag}[1,\ 1,\ \ldots,\ 1]$, and each element of $\boldsymbol{f}$ is a linear combination of zero-mean, independent, and identically distributed random variables (i.e., elements of $\boldsymbol{h}$) with the combining weights determined by the unitary matrix $\boldsymbol{U}$. Although this key observation is deduced based on the equal-power assumption for different paths, it also holds true for practical UWB indoor channels. As a visual proof, Fig. 1 compares the simulated histogram of an element of $\boldsymbol{f}$ with the pdf of a zero-mean unit-variance Gaussian random variable for $L = 2$, $M = 3$ $(LM = 6)$ and a typical standard deviation of 5 dB for $20\log_{10}\alpha(l)$ across $l = 0, \ldots, L-1$. It can be seen from this figure that $\boldsymbol{f}$ can be indeed modeled as zero mean Gaussian. As the LM value increases $(LM > 6)$, the approximation is even more accurate. Therefore, $\boldsymbol{f}$ will be treated as a Gaussian vector with a mean $\boldsymbol{\mu}_f = \boldsymbol{0}_{LM\times 1}$ and a covariance matrix $\boldsymbol{R}_f = \boldsymbol{I}_{LM}$, where $\boldsymbol{0}$ is a vector with all zero elements. Clearly, with such an approximation on the pdf of $\boldsymbol{f}$, γ_p' is equal to a weighted (by the eigenvalues of $\boldsymbol{G}$) sum of independent central chi-square variables, yielding

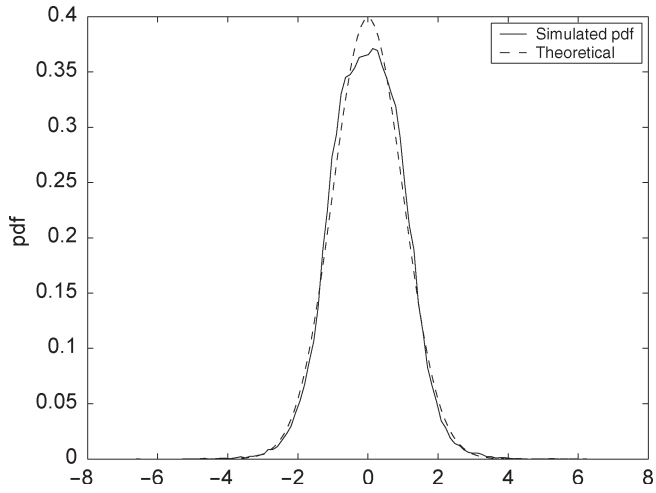

Fig. 1. Approximated pdf of $\boldsymbol{f}$: $L = 2$, $M = 3$, and the standard deviation of $20log_{10}\alpha(l)$ equals 5 dB.

$$\gamma_p' = \sum_{i=1}^{LM} \lambda_i f_i^2 \tag{23}$$

where $f_i,\ \ i = 1, \ldots, LM,$ are zero-mean unit-variance Gaussian random variables.

Because the matrix $\boldsymbol{G}$ depends on the channel fading coefficients, one would expect that its eigenvalues, $\lambda_i,\ i = 1, \cdots, LM$, are random and thus difficult to obtain analytically. It was shown in [9] that the eigenvalues of $\boldsymbol{G}(l)$ are either 1 or 0 with exactly $d = M - N + 1$ eigenvalues equal to 1. Therefore, the matrix $\boldsymbol{G} = \text{diag}[\boldsymbol{G}(0)\ \cdots\ \boldsymbol{G}(L-1)]$ has LM eigenvalues among which $L(M-N+1)$ eigenvalues equal to 1 and the other $L(N-1)$ eigenvalues equal to 0. If these eigenvalues $(\lambda_1,\ \cdots,\ \lambda_{LM})$ are arranged in descending order, we can write

$$[\lambda_1,\ \ldots,\ \lambda_{LM}] = \left[\underbrace{1\ \cdots\ 1}_{L(M-N+1)}\ \underbrace{0\ \cdots\ 0}_{L(N-1)}\right]. \tag{24}$$

With (24), (23) reduces to $\gamma_p' = \sum_{i=1}^{d} f_i^2$, where $d = L(M - N + 1)$. Since f_i is distributed as $f_i \sim \mathcal{N}(0,1)$, the variable γ_p' is a central chi-square distributed random variable with d degrees of freedom and has a pdf expressed as [22]

$$p_{\gamma_p'}(y) = \frac{1}{2^{\frac{d}{2}}\Gamma\left(\frac{1}{2}d\right)} y^{\frac{d}{2}-1} e^{-\frac{y}{2}} \tag{25}$$

where $\Gamma(\cdot)$ is the gamma function defined as $\Gamma(a) = \int_0^\infty \tau^{a-1}e^{-\tau}d\tau,\ a > 0$.

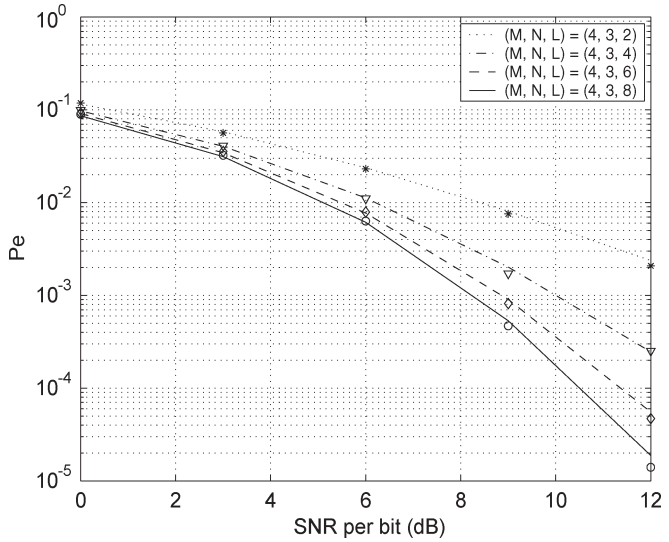

Fig. 2. BER versus SNR per bit for different values of L.

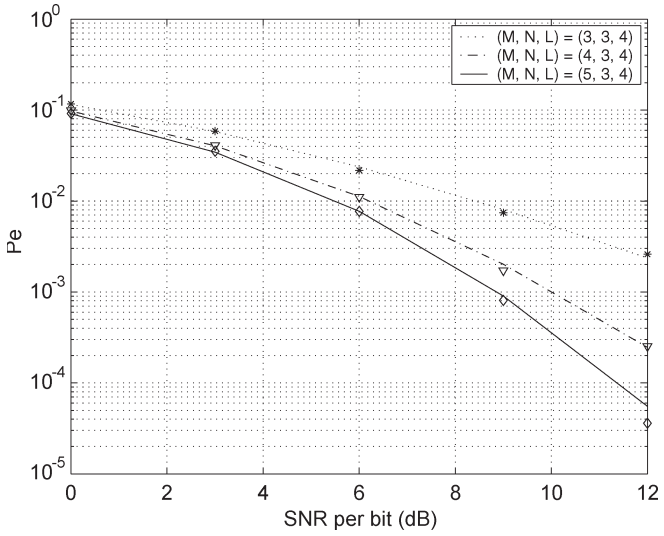

Fig. 3. BER versus SNR per bit for different values of M.

Because $\gamma_p = \gamma_0 \gamma_p'$, the conditional probability of error $P(\gamma_p)$ in (15) is also a function of γ_p'. The average BER in a log-normal fading channel can be computed by averaging $P(\gamma_p')$ over $p(\gamma_p')$ as

$$P_b = \int_0^\infty P(y) p_{\gamma_p'}(y) dy. \tag{26}$$

This BER expression captures any MIMO structure (M, N, L) by a single degree-of-freedom parameter d, which is exactly the diversity order of the corresponding MIMO system. In its simple form, (26) asymptotically approaches the error performance of an optimum UWB MIMO receiver in the high SNR region.

V. Numerical Results and Discussion

As in Section IV, the binary PAM scheme is considered and a 5-dB standard deviation of the channel fading magnitudes is applied in all simulation tests. The average power of the path with index $l = 0$ is assumed to be normalized to unity (i.e., $\Omega_0 = 1$). For the general case that $M \geq N \geq 1$, $L \geq 1$, the SNR per bit in decibel is defined as $\gamma_b = E_b/N_0(\text{dB}) + 10log_{10}[L(M - N + 1)]$. The log-normal fading amplitude $\alpha(l)$ is generated as follows. First, $\alpha(l)$ is expressed as $\alpha(l) = e^{\theta(l)}$, where $\theta(l)$ is a Gaussian random variable with mean $\mu_{\theta(l)}$ and variance σ_θ^2 (independent of l). The kth moment of $\alpha(l)$ is given as $E\{\alpha(l)^k\} = e^{k\mu_{\theta(l)} + k^2\sigma_\theta^2/2}$. To satisfy $E\{\alpha(l)^2\} = e^{-\rho l}$, it is required that $\mu_{\theta(l)} = -\sigma_\theta^2 - \rho l/2$, where σ_θ is obtained as $\sigma_\theta = 5/(20log_{10}e) \approx 0.57$ dB. The receiver is assumed to have perfect knowledge of the channel coefficients.

In all simulations, detection of s_n follows exactly the processing given in (7), (8), and (13). For a MIMO system with $(M, N) = (4, 3)$, the analytical and simulated (with markers) curves of the BER P_b versus bit SNR γ_b are shown in Fig. 2 for various numbers of paths combined by the receiver. In general, the analytical error rates match well the simulated error rates for the set of parameters chosen, although they appear to be slightly worse than the simulated ones. This is caused by approximating $\boldsymbol{f}$ as a Gaussian random vector as in (22). When σ_x and LM are small (e.g., $LM < 6$), the analytical BER values become inaccurate.

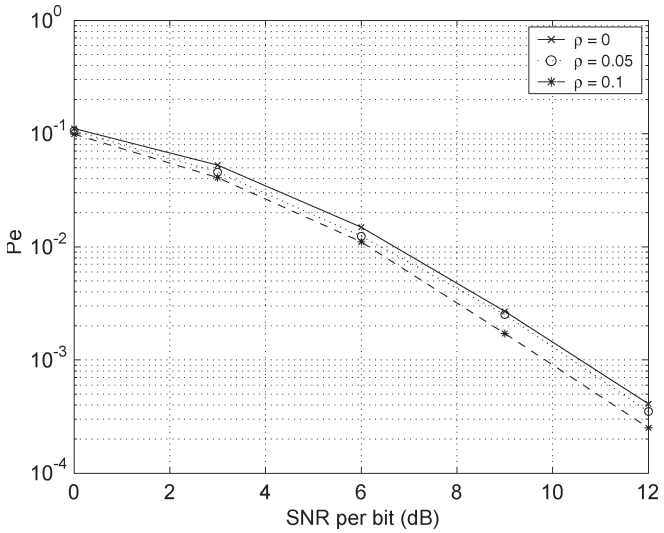

Fig. 4. Impact of ρ ($M = 4$, $N = 3$, $L = 4$).

Fig. 3 shows the BER versus the number of receive antennas M with $N = 3$ and $L = 4$. By examining the slopes of the BER curves, we found that increasing the number of receive antennas M increases the diversity order of the receiver. It is also found that the analytical BER curves for $(M, N, L) = (3, 3, 4)$ and $(M, N, L) = (4, 3, 2)$ are almost the same. This is because that with $\rho = 0$, the diversity order $(L(M - N + 1))$ for these two cases is exactly the same. Thus, with the definition of bit SNR γ_b adopted in this paper, it should yield the same performance.

In the analytical performance evaluation, the power decay factor $\rho = 0$ has been assumed. To justify this assumption, simulated BER versus average SNR per bit γ_b with different ρ values is shown in Fig. 4 for parameters $(M, N, L) = (4, 3, 4)$. A typical value of ρ is obtained to be around 0.056 for a UWB channel with a path resolution $\mathcal{T}_p = 0.2$ ns and a delay spread

$\tau_{\rm rms} = 25$ ns. From Fig. 4, it is shown that the system works slightly better over a channel with $\rho = 0$ than one with $\rho = 0.1$. This is because that with $\rho = 0$ all paths have equal average power, whereas with $\rho = 0.1$ these paths have different average powers. It should be pointed out that the analytical performance with the approximation of $\rho = 0$ becomes more optimistic when the number of paths combined (L) increases. However, combining more than a few paths may significantly increase the receiver complexity. Thus, the analytical performance results can be applied for most practical scenarios.

VI. Conclusion

Analysis of the error performance of an UWB MIMO antenna system over indoor log-normal fading channels has been provided. The receiver consists of a ZF spatial unit that operates on a path-by-path basis and a RAKE temporal combiner that captures L ZF paths. The probability of error is derived, which is expressed as a function of E_b/N_0, the number of transmit and receive antennas, and the number of resolvable paths combined. The analytical error rate expressions can be used to predict the performance of most pulse-based UWB MIMO systems with practical system parameters. It has been observed that under some channel conditions, an (N, M, L) UWB system with $M \geq N$ provides an N-fold throughput of a single-antenna UWB system and at the same time a diversity order of $L(M - N + 1)$ is achieved for each data stream when LM is large.

References

[1] S. Roy, J. R. Foerster, V. S. Somayazulu, and D. G. Leeper, "Ultra-wideband radio design: The promise of high-speed, short-range wireless connectivity," *Proc. IEEE*, vol. 92, no. 2, pp. 295–311, Feb. 2004.

[2] M. Z. Win and R. A. Scholtz, "On the robustness of ultra-wide bandwidth signals in dense multipath environments," *IEEE Commun. Lett.*, vol. 2, no. 2, pp. 51–53, Feb. 1998.

[3] J. R. Foerster, "The effects of multipath interference on the performance of UWB systems in an indoor wireless channel," in *Proc. IEEE Vehicular Technology Conf. (VTC)—Spring*, Rhodes, Greece, 2001, vol. 2, pp. 1176–1180.

[4] R. C. Qiu, "A generalized time domain multipath channel and its applications in ultra-wideband (UWB) wireless optimal receiver design," *IEEE Trans. Wireless Commun.*, to be published.

[5] ——, "A theoretical study of the ultra-wideband wireless propagation channel and optimum UWB receiver design," *IEEE J. Sel. Areas Commun. Special Issue on UWB Multiple Access Communications*, vol. 20, no. 12, pp. 1628–1637, Dec. 2002.

[6] H. Liu, "Error performance of a pulse amplitude and position modulated ultra-wideband system over lognormal fading channels," *IEEE Commun. Lett.*, vol. 7, no. 11, pp. 531–533, Nov. 2003.

[7] Z. Tian and G. B. Giannakis, "BER sensitivity to mistiming in ultra-wideband impulse radios—Part I: Nonrandom channels," *IEEE Trans. Signal Process.*, vol. 53, no. 4, pp. 1550–1560, Apr. 2005.

[8] Z. Tian, L. Yang, and G. B. Giannakis, "Symbol timing estimation in ultra wideband communications," in *Proc. 36th IEEE Asilomar Conf. Signals, Systems, and Computers*, Pacific Grove, CA, Nov. 2002, pp. 1924–1928.

[9] J. H. Winters, J. Salz, and R. D. Gitlin, "The impact of antenna diversity on the capacity of wireless communications systems," *IEEE Trans. Commun.*, vol. 42, no. 2–4, pp. 1740–1751, Feb.–Apr. 1994.

[10] J. H. Winters, "On the capacity of radio communication systems with diversity in a Rayleigh fading environment," *IEEE J. Sel. Areas Commun.*, vol. SAC-5, no. 5, pp. 871–878, Jun. 1987.

[11] G. J. Foschini and M. J. Gans, "On limits of wireless communications in a fading environment when using multiple antennas," *Wireless Pers. Commun.*, vol. 6, no. 3, pp. 311–335, Mar. 1998.

[12] R. S. Blum, J. H. Winters, and N. R. Sollenberger, "On the capacity of cellular systems with MIMO," *IEEE Commun. Lett.*, vol. 6, no. 6, pp. 242–244, Jun. 2002.

[13] G. D. Golden, C. J. Foschini, R. A. Valenzuela, and P. W. Wolniansky, "Detection algorithm and initial laboratory results using V-blast space–time communication architecture," *Electron. Lett.*, vol. 35, no. 1, pp. 14–16, Jan. 1999.

[14] M. Weisenhorn and W. Hirt, "Performance of binary antipodal signaling over the indoor UWB MIMO channel," in *Proc. IEEE Int. Conf. Communications (ICC)*, Anchorage, AK, May 2003, vol. 4, pp. 2872–2878.

[15] M. Biagi and E. Baccarelli, "A simple multiple-antenna ultra wide band transceiver scheme for 4th generation WLAN," in *Proc. IEEE Vehicular Technology Conf. (VTC)*, Orlando, FL, Oct. 2003, vol. 3, pp. 1903–1907.

[16] S. Tan, B. Kannan, and A. Nallanathan, "Performance of UWB multiple access impulse radio systems in multipath environment with antenna array," in *Proc. IEEE Global Telecommunications (GLOBECOM)*, San Francisco, CA, Dec. 2003, vol. 4, pp. 2182–2186.

[17] R. J. Cramer, M. Z. Win, and R. A. Scholtz, "Impulse radio multipath characteristics and diversity reception," in *Proc. IEEE Int. Conf. Communications (ICC)*, Atlanta, GA, 1998, vol. 3, pp. 1650–1654.

[18] H. Hashemi, "Impulse response modeling of indoor radio propagation channels," *IEEE J. Sel. Areas Commun.*, vol. 11, no. 7, pp. 967–978, Sep. 1993.

[19] A. F. Molisch, J. R. Foerster, and M. Pendergrass, "Channel models for ultra-wideband personal area networks," *IEEE Wireless Commun.*, vol. 10, no. 6, pp. 14–21, Dec. 2003.

[20] D. Cassioli, M. Z. Win, and A. F. Molisch, "The ultra-wide bandwidth indoor channel: From statistical model to simulations," *IEEE J. Sel. Areas Commun.*, vol. 20, no. 6, pp. 1247–1257, Aug. 2002.

[21] M. Schwartz, W. R. Bennett, and S. Stein, *Communication Systems and Techniques (Appendix B)*. Piscataway, NJ: IEEE Press, 1995.

[22] J. G. Proakis, *Digital Communications*, 3rd ed. New York: McGraw-Hill, 1995, ch. 14.